Doping dependence of the electronic structure and magnetic order in high-T_c superconductors

B. H. Bernhard and J. R. Iglesias
Instituto de Física, Universidade Federal do Rio Grande do Sul, Caixa Postal 15051, 91501-970 Porto Alegre, RS, Brazil
(Received 28 February 1994; revised manuscript received 6 June 1994)

The local densities of states of an extended Hubbard model describing the CuO_2 planes of superconducting cuprates are calculated by means of an approximate treatment that divides the lattice into CuO_2 clusters. The exact diagonalization of the Hamiltonian on these trimers is utilized to solve the lattice problem, where the hopping between different trimers is treated as a perturbation. The hole concentrations on both orbitals and the amplitude of the staggered magnetization are obtained as a function of the total number of holes. The overall shape of the band structure is in good agreement with exact diagonalization on larger clusters. The stoichiometric compound is found to be metallic in the paramagnetic phase, but becomes a charge-transfer insulator in the antiferromagnetic phase. Electron and hole doping introduce a new band at the bottom or at the top of the charge-transfer gap, respectively. Magnetic order is destroyed when the antiferromagnetic phase becomes unstable against the paramagnetic phase.

I. INTRODUCTION

After intense theoretical and experimental research on the high-T_c superconducting cuprates, it is widely accepted that their peculiar electronic properties arise from the common CuO_2 planes. In particular, the relevant orbitals are $3d_{x^2-y^2}$ for copper and $2p_{x,y}$ for oxygen. These oxides are insulating in the stoichiometric phase, and the copper sublattice exhibits antiferromagnetic order.[1,2] The effect of doping is to introduce carriers into the planes, inducing high-T_c superconductivity.

Both local electronic correlations and covalency are taken into account in the three-band Hubbard Hamiltonian,[3,4] which provides a realistic description of these compounds. The doping dependence of hole distribution and the fast disappearence of antiferromagnetic (AF) long-range order under doping[5–8] have been studied by means of different approaches, namely, the Hartree-Fock approximation,[9] the local ansatz method,[10] a mean-field approximation that includes the disorder introduced by holes,[11] and mean-field slave-boson techniques.[12,13] Also, in Ref. 12, a band was found into the charge-transfer (CT) gap.

A discussion of the doping dependence of the observed spectral weight transfer[14–17] and the distinction between Mott-Hubbard and charge-transfer systems is given by Eskes, Meinders, and Sawatzky,[18] based on the exact diagonalization of one-dimensional clusters. References 19–23 explore the mapping to a t-J model and a one-band Hubbard model. The dynamics of charge carriers has been studied in the context of these simplified versions.[24–27]

The ground-state energy of the three-band Hubbard Hamiltonian on different clusters (up to eight unit cells) has been computed by applying the Lanczos algorithm for numerical diagonalization.[28–30] Holes are shown to bind when the nearest-neighbor Cu-O repulsion is included. Dopf *et al.*[31] calculated the spectral density of the model in the presence of hole doping assuming local correlations only on the copper sites. They applied exact diagonalization to a cluster with 2×2 unit cells and a quantum Monte Carlo approach to a 4×4 cluster. The results show that the Zhang-Rice state forms a dispersive band crossing the Fermi energy. Lanczos and Monte Carlo studies of the three-band Hubbard Hamiltonian have also been carried out by Scalettar *et al.*,[32] who found that the AF correlations decrease with either electron or hole doping, and that the additional holes (electrons) go primarily to the O (Cu) sites.

The one-particle spectral densities on a Cu_4O_8 cluster (including interatomic correlations) have been calculated numerically by Balseiro, Avignon, and Gagliano.[33] The exact diagonalization on a Cu_4O_{13} cluster performed by Maekawa, Ohta, and Tohyama[34] provides reliable informations about the electronic states of the model. In particular, the CT gap is redefined by the presence of the Zhang-Rice (ZR) singlet band, and an in-gap band is formed upon carrier doping.

A current shortcoming in finite-size system calculations is that the band structure arises from Lorentzian broadening of the electronic levels, so that the band edges are not well defined. A more proper broadening should take into account the lattice geometry, not only inside the basic cluster but also among the different clusters.

In this paper we develop an approximate solution of the three-band Hubbard model in which the two-dimensional lattice is considered as a periodic array of CuO_2 clusters (trimers), and the hopping between different trimers is treated perturbatively. The calculated local densities of states on Cu and O sites consist of a number of narrow bands with typical two-dimensional shape. These bands arise from the energy levels of an isolated trimer, which are obtained through exact diagonalization. In order to study the effect of doping, we concentrate on the

trimer expansion, and define a simple interpolation to span all values of hole concentrations. The overall band structures of the stoichiometric and doped systems are quite similar to those of the Cu_4O_{13} cluster.[34] An effect of doping is to introduce new states inside the CT gap. We calculate the hole concentrations on Cu and O sites and the position of the chemical potential as a function of the total number of holes per trimer n in the paramagnetic (PM) and AF phases. For the stoichiometric system, the PM phase is found to be metallic, whereas the AF phase is insulating. The disruption of AF order with doping is studied by calculating the internal energies in both phases. The critical values are consistent with experimental findings.[5–8]

The validity of the present approximation has been recently examined for the one-band Hubbard model on a dimerized square lattice.[35] where we concentrated on the paramagnetic half-filled-band case and considered the effect of temperature. Here, in the CuO_2 lattice, the physics is mainly governed by the charge transfer between the two orbitals involved, and the more relevant questions concern the doping dependence, so we will restrict ourselves to the zero temperature limit.

In the next section, we present the model Hamiltonian and apply a Green function technique to obtain the local spectral functions of the PM phase. In Sec. III, an AF solution is considered. Results are discussed in Sec. IV.

II. TRIMERS LATTICE APPROACH

We write the three-band Hubbard Hamiltonian in a modified notation, with reference to the trimers lattice of Fig. 1.

$$\mathcal{H} = \sum_{i\alpha\sigma} (\mathcal{H}^0_{i\alpha\sigma} + V_{i\alpha\sigma}), \tag{1}$$

where

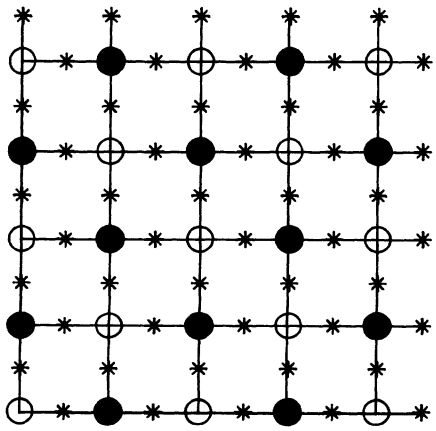

FIG. 1. The CuO_2 lattice. Stars represent O sites; white and black circles are Cu sites with up and down magnetic moments, respectively.

$$\begin{aligned}\mathcal{H}^0_{i\alpha\sigma} = {} & (\Delta - \mu)(n^a_{i\alpha\sigma} + n^c_{i\alpha\sigma}) - \mu\, n^d_{i\alpha\sigma} \\ & + \tfrac{1}{2}U_d n^d_{i\alpha\uparrow} n^d_{i\alpha\downarrow} + \tfrac{1}{2}U_p (n^a_{i\alpha\uparrow} n^a_{i\alpha\downarrow} + n^c_{i\alpha\uparrow} n^c_{i\alpha\downarrow}) \\ & - t(a^\dagger_{i\alpha\sigma} d_{i\alpha\sigma} + d^\dagger_{i\alpha\sigma} a_{i\alpha\sigma} - c^\dagger_{i\alpha\sigma} d_{i\alpha\sigma} - d^\dagger_{i\alpha\sigma} c_{i\alpha\sigma})\end{aligned} \tag{2}$$

and

$$\begin{aligned}V_{i\alpha\sigma} = {} & -t(c^\dagger_{i\alpha\sigma} d_{i+1,\alpha,\sigma} - a^\dagger_{i\alpha\sigma} d_{i,\alpha+1,\sigma} \\ & + d^\dagger_{i\alpha\sigma} c_{i-1,\alpha,\sigma} - d^\dagger_{i\alpha\sigma} a_{i,\alpha-1,\sigma}).\end{aligned} \tag{3}$$

The pair of indices $i\alpha$ give the position of each trimer on a square lattice. $b^\dagger_{i\alpha\sigma}$ ($b_{i\alpha\sigma}$) is the operator that creates (annihilates) a hole with spin σ on a "b" site of the trimer $i\alpha$ (b= a or c for the oxygen sites, or d for the copper site), and $n^b_{i\alpha\sigma} = b^\dagger_{i\alpha\sigma} b_{i\alpha\sigma}$. Δ is the energy difference between p and d orbitals, U_d and U_p are the Coulomb repulsive interactions on copper and oxygen ions, respectively, and t is the hopping between neighboring p and d orbitals.

The first step is the exact diagonalization of $\mathcal{H}^0_{i\alpha} = \sum_\sigma \mathcal{H}^0_{i\alpha\sigma}$. The largest size, 4×4, of the irreducible matrices involved can be further reduced to 3×3 if we make the simple assumption $U_d = U_p + 2\Delta$, which is not far from realistic parameter values. The eigenvalues and eigenvectors of the Hamiltonian $\mathcal{H}^0_{i\alpha}$ in the subspaces of 0, 1, 2, and 3 particles are shown in Table I, where we make use of the definitions

$$\tan\theta_1 = \frac{\Delta + R_1}{2t\sqrt{2}}, \tag{4}$$

$$\tan\theta_2 = \frac{\Delta + U_p + R_2}{2t\sqrt{2}}, \tag{5}$$

$$\tan\phi_{2,i} = \frac{1}{\sqrt{3}} \frac{2\Delta + U_p - \lambda_i}{2\Delta - \lambda_i}, \tag{6}$$

$$\tan\theta_{2,i} = \frac{2\Delta + U_p - \lambda_i}{t\sqrt{6}} \cos\phi_{2,i}, \tag{7}$$

$$R_1 = \sqrt{\Delta^2 + 8t^2}, \tag{8}$$

$$R_2 = \sqrt{(\Delta + U_p)^2 + 8t^2}, \tag{9}$$

and λ_i ($i = 1, 6, 9$) are the roots of the cubic equation

$$(2\Delta - \lambda)(2\Delta + U_p - \lambda)(\Delta - \lambda) = 2t^2(8\Delta + U_p - 4\lambda). \tag{10}$$

The particular case $\Delta = 0$, $U_d = U_p$ corresponds to the one-band Hubbard model and was considered in Ref. 36.

The trimer's Green functions $g^{(n)}_{bb'}(\omega)$ for fixed number of particles n (= 0, 1, or 2) per unit cell are obtained by the spectral representation, after evaluation of all matrix elements involving the corresponding ground state $|(n)\rangle$. They can be written in the form

TABLE I. Eigenvalues and eigenvectors of $\mathcal{H}_0$ for 0, 1, 2, and 3 particles.

$E_0 = 0$	$\|0\rangle$
$E_{1,1} = \frac{1}{2}(\Delta - R_1) - \mu$	$\|1,1\sigma\rangle = \sin\theta_1 d^\dagger_\sigma + \frac{\cos\theta_1}{\sqrt{2}}(a^\dagger_\sigma - c^\dagger_\sigma)\|0\rangle$
$E_{1,2} = \Delta - \mu$	$\|1,2\sigma\rangle = \frac{1}{\sqrt{2}}(a^\dagger_\sigma + c^\dagger_\sigma)\|0\rangle$
$E_{1,3} = \frac{1}{2}(\Delta + R_1) - \mu$	$\|1,3\sigma\rangle = -\cos\theta_1 d^\dagger_\sigma + \frac{\sin\theta_1}{\sqrt{2}}(a^\dagger_\sigma - c^\dagger_\sigma)\|0\rangle$
$E_{2,i} = \lambda_i - 2\mu \quad (i = 1,6,9)$	$\|2,i\rangle = \frac{\sin\theta_{2,i}}{2}\left(a^\dagger_\uparrow d^\dagger_\downarrow - c^\dagger_\uparrow d^\dagger_\downarrow - a^\dagger_\downarrow d^\dagger_\uparrow + c^\dagger_\downarrow d^\dagger_\uparrow\right)\|0\rangle$ $+\frac{\cos\theta_{2,i}\sin\phi_{2,i}}{\sqrt{2}}\left(a^\dagger_\uparrow c^\dagger_\downarrow - a^\dagger_\downarrow c^\dagger_\uparrow\right)\|0\rangle$ $-\frac{\cos\theta_{2,i}\cos\phi_{2,i}}{\sqrt{6}}\left(a^\dagger_\uparrow a^\dagger_\downarrow + c^\dagger_\uparrow c^\dagger_\downarrow + 2d^\dagger_\uparrow d^\dagger_\downarrow\right)\|0\rangle$
$E_{2,2} = \frac{1}{2}(3\Delta + U_p - R_2) - 2\mu$	$\|2,2\rangle = \frac{\cos\theta_2}{\sqrt{2}}\left(a^\dagger_\uparrow a^\dagger_\downarrow - c^\dagger_\uparrow c^\dagger_\downarrow\right)\|0\rangle + \frac{\sin\theta_2}{2}\left(a^\dagger_\uparrow d^\dagger_\downarrow - a^\dagger_\downarrow d^\dagger_\uparrow + c^\dagger_\uparrow d^\dagger_\downarrow - c^\dagger_\downarrow d^\dagger_\uparrow\right)\|0\rangle$
$E_{2,3} = \frac{1}{2}(3\Delta - R_1) - 2\mu$	$\|2,3\rangle = -\frac{\cos\theta_1}{\sqrt{2}}\left(a^\dagger_\uparrow c^\dagger_\downarrow + a^\dagger_\downarrow c^\dagger_\uparrow\right)\|0\rangle + \frac{\sin\theta_1}{2}\left(a^\dagger_\uparrow d^\dagger_\downarrow + a^\dagger_\downarrow d^\dagger_\uparrow + c^\dagger_\uparrow d^\dagger_\downarrow + c^\dagger_\downarrow d^\dagger_\uparrow\right)\|0\rangle$
	$\|2,3\sigma\rangle = -\cos\theta_1 a^\dagger_\sigma c^\dagger_\sigma\|0\rangle + \frac{\sin\theta_1}{\sqrt{2}}\left(a^\dagger_\sigma d^\dagger_\sigma + c^\dagger_\sigma d^\dagger_\sigma\right)\|0\rangle$
$E_{2,4} = \Delta - 2\mu$	$\|2,4\rangle = \frac{1}{2}\left(a^\dagger_\uparrow d^\dagger_\downarrow + a^\dagger_\downarrow d^\dagger_\uparrow - c^\dagger_\uparrow d^\dagger_\downarrow - c^\dagger_\downarrow d^\dagger_\uparrow\right)\|0\rangle$
	$\|2,4\sigma\rangle = \frac{1}{\sqrt{2}}\left(a^\dagger_\sigma d^\dagger_\sigma - c^\dagger_\sigma d^\dagger_\sigma\right)\|0\rangle$
$E_{2,5} = 2\Delta + U_p - 2\mu$	$\|2,5\rangle = \frac{1}{\sqrt{3}}\left(a^\dagger_\uparrow a^\dagger_\downarrow + c^\dagger_\uparrow c^\dagger_\downarrow - d^\dagger_\uparrow d^\dagger_\downarrow\right)\|0\rangle$
$E_{2,7} = \frac{1}{2}(3\Delta + R_1) - 2\mu$	$\|2,7\rangle = \frac{\sin\theta_1}{\sqrt{2}}\left(a^\dagger_\uparrow c^\dagger_\downarrow + a^\dagger_\downarrow c^\dagger_\uparrow\right)\|0\rangle + \frac{\cos\theta_1}{2}\left(a^\dagger_\uparrow d^\dagger_\downarrow + a^\dagger_\downarrow d^\dagger_\uparrow + c^\dagger_\uparrow d^\dagger_\downarrow + c^\dagger_\downarrow d^\dagger_\uparrow\right)\|0\rangle$
	$\|2,7\sigma\rangle = \sin\theta_1 a^\dagger_\sigma c^\dagger_\sigma\|0\rangle + \frac{\cos\theta_1}{\sqrt{2}}\left(a^\dagger_\sigma d^\dagger_\sigma + c^\dagger_\sigma d^\dagger_\sigma\right)\|0\rangle$
$E_{2,8} = \frac{1}{2}(3\Delta + U_p + R_2) - 2\mu$	$\|2,8\rangle = -\frac{\sin\theta_2}{\sqrt{2}}\left(a^\dagger_\uparrow a^\dagger_\downarrow - c^\dagger_\uparrow c^\dagger_\downarrow\right)\|0\rangle + \frac{\cos\theta_2}{2}\left(a^\dagger_\uparrow d^\dagger_\downarrow - a^\dagger_\downarrow d^\dagger_\uparrow + c^\dagger_\uparrow d^\dagger_\downarrow - c^\dagger_\downarrow d^\dagger_\uparrow\right)\|0\rangle$
$E_{3,i} = 4\Delta + U_p - \lambda_i - 3\mu \quad (i = 1,6,9)$	$\|3,i\sigma\rangle = -\frac{\sin\theta_{2,i}}{2}\left(a^\dagger_\sigma a^\dagger_{\bar\sigma} c^\dagger_\sigma + a^\dagger_\sigma d^\dagger_\sigma d^\dagger_{\bar\sigma} + d^\dagger_\sigma d^\dagger_{\bar\sigma} c^\dagger_\sigma + a^\dagger_\sigma c^\dagger_\sigma c^\dagger_{\bar\sigma}\right)\|0\rangle$ $+\frac{\cos\theta_{2,i}\sin\phi_{2,i}}{\sqrt{2}}\left(d^\dagger_\sigma c^\dagger_\sigma c^\dagger_{\bar\sigma} - a^\dagger_\sigma a^\dagger_{\bar\sigma} d^\dagger_\sigma\right)\|0\rangle$ $-\frac{\cos\theta_{2,i}\cos\phi_{2,i}}{\sqrt{6}}\left(a^\dagger_\sigma d^\dagger_\sigma c^\dagger_{\bar\sigma} + a^\dagger_{\bar\sigma} d^\dagger_\sigma c^\dagger_\sigma - 2a^\dagger_\sigma d^\dagger_{\bar\sigma} c^\dagger_\sigma\right)\|0\rangle$
$E_{3,2} = \frac{1}{2}(5\Delta + U_p - R_2) - 3\mu$	$\|3,2\sigma\rangle = \frac{\cos\theta_2}{2}\left(a^\dagger_\sigma a^\dagger_{\bar\sigma} c^\dagger_\sigma - a^\dagger_\sigma d^\dagger_\sigma d^\dagger_{\bar\sigma} + d^\dagger_\sigma d^\dagger_{\bar\sigma} c^\dagger_\sigma - a^\dagger_\sigma c^\dagger_\sigma c^\dagger_{\bar\sigma}\right)\|0\rangle$ $+\frac{\sin\theta_2}{\sqrt{2}}\left(a^\dagger_\sigma d^\dagger_\sigma c^\dagger_{\bar\sigma} - a^\dagger_{\bar\sigma} d^\dagger_\sigma c^\dagger_{\bar\sigma}\right)\|0\rangle$
$E_{3,3} = \frac{1}{2}(5\Delta - R_1) + U_p - 3\mu$	$\|3,3\sigma\rangle = \frac{\cos\theta_1}{2}\left(a^\dagger_\sigma a^\dagger_{\bar\sigma} c^\dagger_\sigma + a^\dagger_\sigma d^\dagger_\sigma d^\dagger_{\bar\sigma} - d^\dagger_\sigma d^\dagger_{\bar\sigma} c^\dagger_\sigma - a^\dagger_\sigma c^\dagger_\sigma c^\dagger_{\bar\sigma}\right)\|0\rangle$ $+\frac{\sin\theta_1}{\sqrt{2}}\left(a^\dagger_\sigma a^\dagger_{\bar\sigma} d^\dagger_\sigma + d^\dagger_\sigma c^\dagger_\sigma c^\dagger_{\bar\sigma}\right)\|0\rangle$
$E_{3,4} = 2\Delta - 3\mu$	$\|3,4\sigma\rangle = \frac{1}{\sqrt{3}}\left(a^\dagger_\sigma d^\dagger_\sigma c^\dagger_{\bar\sigma} + a^\dagger_\sigma d^\dagger_{\bar\sigma} c^\dagger_\sigma + a^\dagger_{\bar\sigma} d^\dagger_\sigma c^\dagger_\sigma\right)\|0\rangle$
	$\|3,4\sigma\sigma\rangle = a^\dagger_\sigma d^\dagger_\sigma c^\dagger_\sigma\|0\rangle$

TABLE I. (*Continued*).

$E_{3,5} = 3\Delta + U_p - 3\mu$	$\|3,5\sigma\rangle = \frac{1}{2}\left(a^\dagger_\sigma a^\dagger_{\bar\sigma} c^\dagger_\sigma - a^\dagger_\sigma d^\dagger_\sigma d^\dagger_{\bar\sigma} - d^\dagger_\sigma d^\dagger_{\bar\sigma} c^\dagger_\uparrow + a^\dagger_\sigma c^\dagger_\sigma c^\dagger_{\bar\sigma}\right)\|0\rangle$
$E_{3,7} = \frac{1}{2}(5\Delta + R_1) + U_p - 3\mu$	$\|3,7\sigma\rangle = \frac{\sin\theta_1}{2}\left(a^\dagger_\sigma a^\dagger_{\bar\sigma} c^\dagger_\sigma + a^\dagger_\sigma d^\dagger_\sigma d^\dagger_{\bar\sigma} - d^\dagger_\sigma d^\dagger_{\bar\sigma} c^\dagger_\sigma - a^\dagger_\sigma c^\dagger_\sigma c^\dagger_{\bar\sigma}\right)\|0\rangle$
	$-\frac{\cos\theta_1}{\sqrt{2}}\left(a^\dagger_\sigma a^\dagger_{\bar\sigma} d^\dagger_\sigma + d^\dagger_\sigma c^\dagger_\sigma c^\dagger_{\bar\sigma}\right)\|0\rangle$
$E_{3,8} = \frac{1}{2}(5\Delta + U_p + R_2) - 3\mu$	$\|3,8\sigma\rangle = \frac{\sin\theta_2}{2}\left(a^\dagger_\sigma a^\dagger_{\bar\sigma} c^\dagger_\sigma - a^\dagger_\sigma d^\dagger_\sigma d^\dagger_{\bar\sigma} + d^\dagger_\sigma d^\dagger_{\bar\sigma} c^\dagger_\sigma - a^\dagger_\uparrow c^\dagger_\sigma c^\dagger_{\bar\sigma}\right)\|0\rangle$
	$-\frac{\cos\theta_2}{\sqrt{2}}\left(a^\dagger_\sigma d^\dagger_\sigma c^\dagger_{\bar\sigma} - a^\dagger_{\bar\sigma} d^\dagger_\sigma c^\dagger_{\bar\sigma}\right)\|0\rangle$

$$g^{(n)}_{bb'} = \sum_l \frac{A^{(n)}_{l,bb'}}{\omega - p_l}, \tag{11}$$

where

$$A^{(n)}_{l,bb'} = \sum_i \Big[\delta_{E_i,E_{(n)}+p_l}\langle i|b^\dagger|(n)\rangle\langle(n)|b'|i\rangle + \delta_{E_i,E_{(n)}-p_l}\langle i|b'|(n)\rangle\langle(n)|b^\dagger|i\rangle\Big], \tag{12}$$

$E_{(n)}$ being the ground-state energy for n particles.

The unperturbed Green functions $g^\sigma_{bb'}$ are expected to be continuous functions of the hole concentration n. The form of such dependence is rather obvious in an atomic expansion, the Hubbard I approximation, where a self-consistency can be straightforwardly defined for both PM and AF solutions.[37–39] For the present trimer expansion, we assume that the hole propagates on an effective lattice composed by two kinds of trimers: one having an integer number n_0 of holes and another with $n_0 + 1$ holes. The concentrations of both trimer species are functions of the average number n of holes per trimer, with $n_0 \le n \le n_0 + 1$. Here we choose a simple, smooth interpolation between n_0 and $n_0 + 1$:

$$g_{bb'} = \begin{cases} (1-n)g^{(0)}_{bb'} + n g^{(1)}_{bb'} & \text{if } 0 \le n \le 1, \\ (2-n)g^{(1)}_{bb'} + (n-1)g^{(2)}_{bb'} & \text{if } 1 < n \le 2, \end{cases} \tag{13}$$

where $b, b' = a, d$, or c. Fractional values of n would be more properly described if one could increase the size of the basic cluster.

The remaining one-particle term, $V_{i\alpha\sigma}$, in (1) is included by assuming Dyson-like equations for the lattice Green functions $G^\sigma_{bb'}(i\alpha; j\beta)$ describing the propagation of an electron from site b' of a given trimer $(j\beta)$ to site b of trimer $(i\alpha)$. Taking into account the symmetry of the lattice, these equations can be grouped in matrix form as

$$\mathbf{G}^\sigma(i\alpha; j\beta) = \delta_{ij}\delta_{\alpha\beta}\mathbf{g}^\sigma_i - \mathbf{g}^\sigma_i\{\mathbf{T}_+\mathbf{G}^\sigma(i+1,\alpha; j\beta) + \tilde{\mathbf{T}}_+\mathbf{G}^\sigma(i-1,\alpha; j\beta) - \mathbf{T}_-\mathbf{G}^\sigma(i,\alpha+1; j\beta) - \tilde{\mathbf{T}}_-\mathbf{G}^\sigma(i,\alpha-1; j\beta)\}, \tag{14}$$

where

$$\mathbf{G}^\sigma = \begin{pmatrix} G^\sigma_{aa} & G^\sigma_{ad} & G^\sigma_{ac} \\ G^\sigma_{da} & G^\sigma_{dd} & G^\sigma_{dc} \\ G^\sigma_{ca} & G^\sigma_{cd} & G^\sigma_{cc}, \end{pmatrix}, \tag{15}$$

$$\mathbf{g}^\sigma_i = \begin{pmatrix} g^\sigma_{aa} & g^\sigma_{ad} & g^\sigma_{ac} \\ g^\sigma_{ad} & g^\sigma_{dd} & -g^\sigma_{ad} \\ g^\sigma_{ac} & -g^\sigma_{ad} & g^\sigma_{aa} \end{pmatrix}, \tag{16}$$

$$\mathbf{T}_+ = \begin{pmatrix} 0 & 0 & 0 \\ 0 & 0 & 0 \\ 0 & t & 0 \end{pmatrix}, \qquad \mathbf{T}_- = \begin{pmatrix} 0 & t & 0 \\ 0 & 0 & 0 \\ 0 & 0 & 0 \end{pmatrix}. \tag{17}$$

Fourier transformation yields

$$\mathbf{G}^\sigma(\mathbf{k}) = [\mathbf{1} + \mathbf{g}^\sigma\mathbf{E}^\sigma(\mathbf{k})]^{-1}\mathbf{g}^\sigma, \tag{18}$$

with

$$\mathbf{E}^\sigma(\mathbf{k}) = t\begin{pmatrix} 0 & e^{ik_y a} & 0 \\ e^{-ik_y a} & 0 & -e^{-ik_x a} \\ 0 & -e^{ik_x a} & 0 \end{pmatrix}, \tag{19}$$

where a is the lattice parameter.

From the inverse transformation,

$$\mathbf{G}^\sigma(i\alpha; j\beta) = \frac{1}{N}\sum_{\mathbf{k}} \mathbf{G}^\sigma(\mathbf{k})e^{-i\mathbf{k}\cdot(\mathbf{R}_{i\alpha} - \mathbf{R}_{j\beta})}, \tag{20}$$

we obtain the local Green functions

$$G^\sigma_{dd} = \frac{g^\sigma_{dd}}{2\pi}\int_{-\pi}^{\pi} \frac{dy}{\sqrt{P(\cos y)}}, \tag{21}$$

$$G^\sigma_{aa} = \frac{1}{2\pi}\int_{-\pi}^{\pi} dy \frac{a_4 + a_5\cos y}{\sqrt{P(\cos y)}}, \tag{22}$$

and

$$G^\sigma_{ad} = \frac{1}{2\pi}\int_{-\pi}^{\pi} dy \frac{g^\sigma_{ad} - t a_6 \cos y}{\sqrt{P(\cos y)}}, \tag{23}$$

where

$$P(x) = a_1 x^2 + a_2 x + a_3, \tag{24}$$

$$a_1 = 4t^2(g^\sigma_{ad})^2, \tag{25}$$
$$a_2 = -4tg^\sigma_{ad}[1 - 2t^2 g_{dd}(g^\sigma_{aa} + g^\sigma_{ac})], \tag{26}$$
$$a_3 = 1 - 4t^2 g^\sigma_{dd} a_4, \tag{27}$$
$$a_4 = g^\sigma_{aa} + t^2(g^\sigma_{aa} + g^\sigma_{ac})a_6, \tag{28}$$
$$a_5 = -2tg_{ad}(g^\sigma_{aa} + g^\sigma_{ac}), \tag{29}$$
$$a_6 = 2(g^\sigma_{ad})^2 + g^\sigma_{dd}(g^\sigma_{ac} - g^\sigma_{aa}). \tag{30}$$

The local densities of states (LDOS) $\rho(\omega)$ on Cu and O sites, shown in Figs. 2, 3, and 4 for $n = 0$, 1, and 2, respectively, arise from the imaginary part of these Green functions, which we obtain by numerical integration of Eqs. (21) and (22). We have chosen the parameter values $\Delta = 2.6t$, $U_p = 4.6t$, and $U_d = 9.8t$. The energy ω is given in units of t and measured with respect to $\Delta/2$. The arrows mark the position of the chemical potential. The different bands originating from the one-particle energy levels of the CuO_2 trimer have typical low-dimensional shape, with logarithmic singularities and sharp band edges leading to well-defined gaps.

In the absence of correlation, the densities of states in Fig. 2 would be filled in a rigid band way. In addition to the hybridized bonding and antibonding bands, there is an oxygen nonbonding band at $\omega = \Delta/2$. Each one of these bands can accommodate up to 2.00 holes. The CT gap E_g conserves its atomic value Δ.

By comparing Fig. 3 to the spectral functions obtained from exact diagonalization on a Cu_4O_{13} cluster,[34]

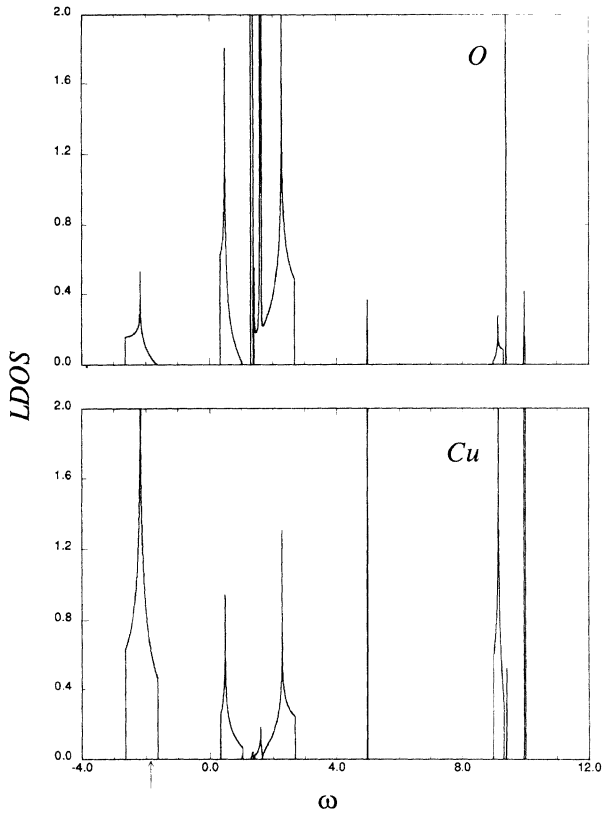

FIG. 3. Same as Fig. 2 but for $n = 1$. The arrow indicates the position of the chemical potential.

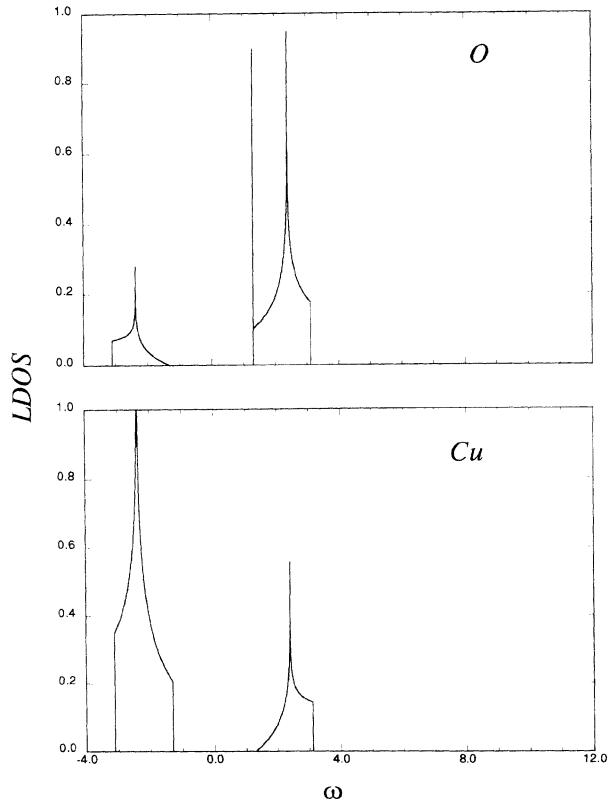

FIG. 2. LDOS on Cu and O sites for $n = 0$ in the PM phase. Units and parameters are specified in the text.

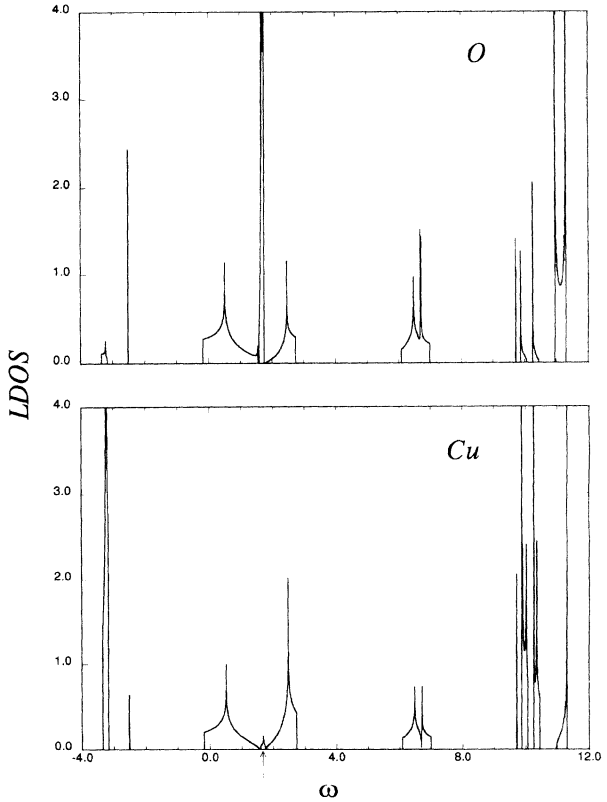

FIG. 4. Same as Fig. 3 but for $n = 2$.

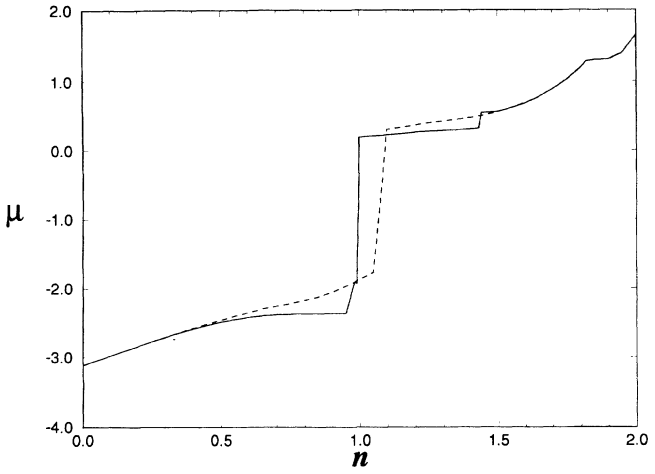

FIG. 5. Chemical potential μ in the PM (dashed) and AF (solid) phases as a function of the total number n of holes per trimer.

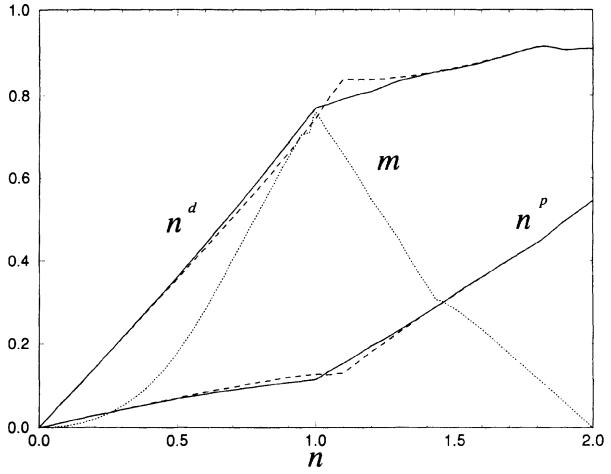

FIG. 6. Hole concentrations on Cu and O sites in the PM (dashed) and AF (solid) phases, and the staggered magnetization (dotted) as a function of the total number n of holes per trimer.

where slightly different parameter values were employed, we find good agreement in the position of the bands. We observe that E_g is reduced by the presence of the band at $\omega \approx 0.7t$, with predominantly O character, which corresponds to the Zhang-Rice singlet band.[34,31,19] Indeed, in our treatment, this band originates from the transition between the trimer's ground state of one particle ($|1,1\sigma\rangle$) and the lowest energy state of two particles ($|2,1\rangle$). In the large U_p (and U_d) limit,

$$|2,1\rangle \rightarrow \frac{1}{\sqrt{2}}\left(\phi_{\uparrow}^{\dagger} d_{\downarrow}^{\dagger} - \phi_{\downarrow}^{\dagger} d_{\uparrow}^{\dagger}\right)|0\rangle, \tag{31}$$

where

$$\phi_{\sigma}^{\dagger} = \frac{1}{\sqrt{2}}\left(a_{\sigma}^{\dagger} - c_{\sigma}^{\dagger}\right). \tag{32}$$

By direct integration one verifies that the total weight of the lower band is ≈ 1.13, so that the chemical potential μ is clearly located below the CT gap.

Inspection of Fig. 4 shows that the width of the lower band decreases monotonically as n increases, whereas the width of the ZR singlet band increases. The very narrow band at $\omega \approx -2.5t$ arises from the pole $E_{2,1} - E_{1,2}$ (see Table I).

For intermediate values of n, we make use of the interpolation defined in Eq. (13). The dashed line in Fig. 5 gives the chemical potential μ (measured from $\Delta/2$) as a function of n. The CT gap corresponds to the discontinuity at $n \approx 1.10$. The doping dependence of the hole concentrations on Cu and O orbitals is shown by the dashed lines in Fig. 6. If the PM phase could be stabilized, practically all doped holes (until the concentration $n \approx 1.10$) would go to the Cu sites.

III. THE ANTIFERROMAGNETIC PHASE

In the AF phase, we define two sublattices, with $\mathbf{g}_j^{\sigma} = \mathbf{g}_i^{\bar{\sigma}}$ for i,j belonging to different sublattices. The "down spin" trimers (marked by black circles in Fig. 1) are eliminated by using Eq. (14). In the new lattice all trimers are equivalent and each one is connected to eight neighbors (its nearest-neighbor and next-nearest-neighbor trimers) through renormalized hopping matrices.

We assume that an infinitesimal magnetic field h resolves the ground-state degeneracy for $n = 1$, so that $g_{bb'}^{(1)}$ is replaced by spin-dependent definitions $g_{bb'}^{(1)\sigma}$. Following the procedure adopted in the nonmagnetic solution, we obtain

$$\mathbf{G}^{\sigma}(\mathbf{k}) = \left[\mathbf{1} + \mathbf{g}_*^{\sigma}\mathbf{E}_*^{\sigma}(\mathbf{k})\right]^{-1}\mathbf{g}_*^{\sigma}, \tag{33}$$

where

$$\mathbf{g}_*^{\sigma} = \left[\mathbf{1} - \mathbf{g}^{\sigma}\mathbf{W}^{\sigma}\right]^{-1}\mathbf{g}^{\sigma}, \tag{34}$$

$$\mathbf{W}^{\sigma} = t^2 \begin{pmatrix} g_{dd}^{\bar{\sigma}} & 0 & 0 \\ 0 & 2g_{aa}^{\bar{\sigma}} & 0 \\ 0 & 0 & g_{dd}^{\bar{\sigma}} \end{pmatrix}, \tag{35}$$

and

$$\mathbf{E}_*^{\sigma}(\mathbf{k}) = t^2 \begin{pmatrix} 0 & -g_{ad}^{\bar{\sigma}} e^{ik_x a'}\left(1 + e^{ik_y a'}\right) & g_{dd}^{\bar{\sigma}} e^{ik_y a'} \\ -g_{ad}^{\bar{\sigma}} e^{-ik_x a'}\left(1 + e^{-ik_y a'}\right) & 2g_{ac}^{\bar{\sigma}} \cos k_y a' & g_{ad}^{\bar{\sigma}} e^{-ik_x a'}\left(1 + e^{ik_y a'}\right) \\ g_{dd}^{\bar{\sigma}} e^{-ik_y a'} & g_{ad}^{\bar{\sigma}} e^{ik_x a'}\left(1 + e^{-ik_y a'}\right) & 0 \end{pmatrix}, \tag{36}$$

with $a' = a\sqrt{2}$.

We can write the following expressions for the local Green functions:

$$G^{\sigma}_{dd} = \frac{1}{\pi C}\left(\lambda'_0 I_0 + \lambda'_1 I_1\right), \tag{37}$$

$$G^{\sigma}_{aa} = \frac{g^{\sigma}_{+}}{2} + \frac{1}{2\pi C}\left(\lambda_0 I_0 + \lambda_1 I_1 + \lambda_2 I_2\right), \tag{38}$$

and

$$G^{\sigma}_{ad} = \frac{F}{2g^{\sigma}_{ad}} + \frac{1}{4\pi g^{\sigma}_{ad} C}\left(\lambda''_0 I_0 + \lambda''_1 I_1 + \lambda''_2 I_2\right), \tag{39}$$

where

$$I_n = \int_{-1}^{1} \frac{y^n dy}{\sqrt{(1-y^2)(r-y)(s-y)(u-y)(v-y)}}. \tag{40}$$

The new quantities appearing above are defined in the Appendix.

The first term in Eq. (38) gives rise to the nonbonding part of the band structure, consisting of a number of δ functions. This term is also present in Eq. (22), although not explicitly.

The LDOS determine the concentrations $\langle n^d_\sigma \rangle$, $\langle n^a_\sigma \rangle$, and also the Fermi energy that corresponds to the given n [$= \sum_\sigma (\langle n^d_\sigma \rangle + 2\langle n^a_\sigma \rangle)$]. Figure 7 shows the calculated spectral functions of the undoped system. Comparing to the PM case in Fig. 3, we observe a narrowing in the lower band. With the new distribution of spectral weight among the bands, the Fermi level falls in the CT gap. Logarthmic singularities are observed at both edges of this gap.

Figures 8 and 9 illustrate the influence of doping on the spectral functions for $n = 0.95$ and $n = 1.01$. Comparing to the stoichiometric LDOS of Fig. 7, we see that electron doping (Fig. 8) produces a new band inside the CT gap near the lower band. For hole doping (Fig. 9), the corresponding band appears at the opposite side of the CT gap, through the splitting of the ZR band. Thus the assumption of the interpolation defined in Eq. (13) produces the same qualitative behavior emerging from cluster diagonalization.[34]

The chemical potential μ as a function of the total number of holes per trimer n is shown by the solid line in Fig. 5. The doping dependence of the Cu($3d$) and O($2d$) hole densities and the magnetization on the Cu sites can be seen in Fig. 6 (solid line). As in the PM phase, doped electrons prefer the Cu ions, but doped holes go mostly to O sites.

Although the AF phase is defined in the whole range of concentrations, we know that magnetic order is destroyed for a sufficiently large amount of doping. Thus one has to examine the relative stability of the two phases we are considering. The internal energy per unit cell can be calculated through

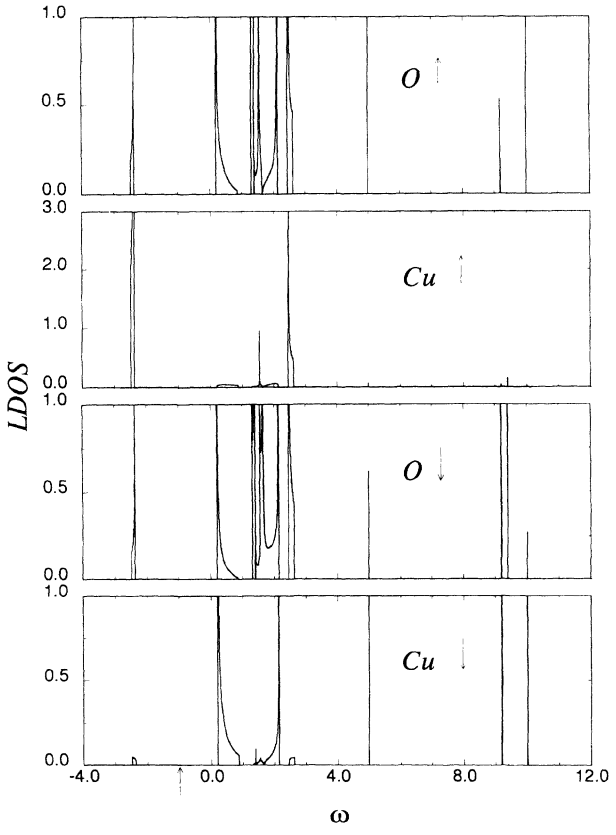

FIG. 7. LDOS for $n = 1.0$ in the AF phase for up and down spin on Cu and O sites.

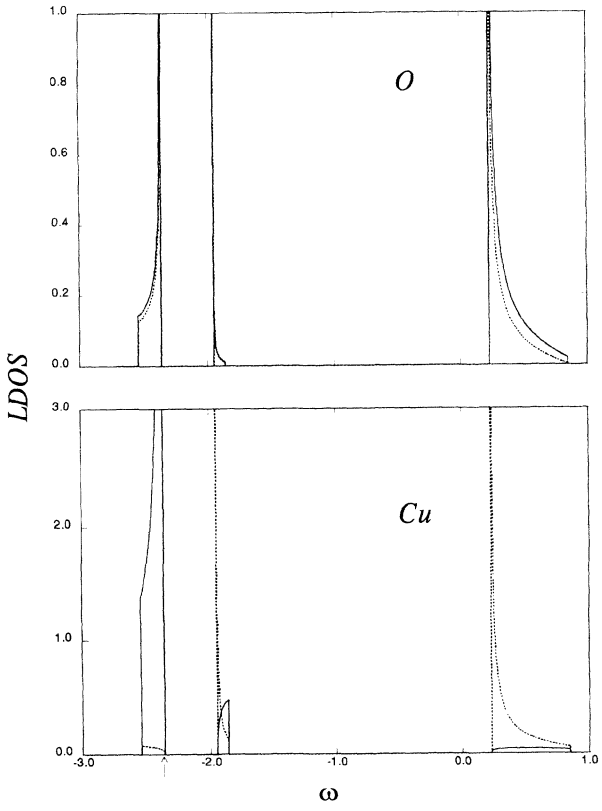

FIG. 8. Low energy part of the LDOS for up and down spin (solid and dashed lines, respectively) on Cu and O sites in the AF phase for $n = 0.95$.

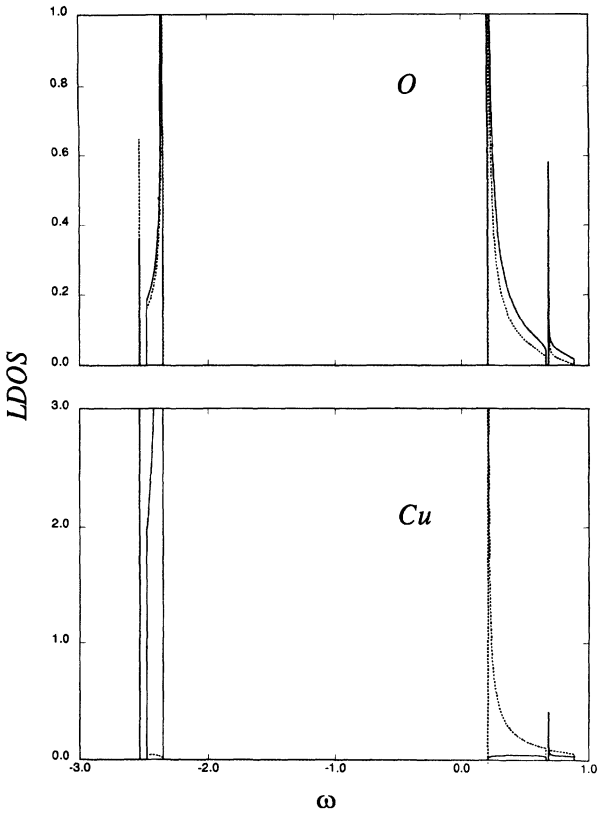

FIG. 9. Same as in Fig. 8 but for $n = 1.01$.

$$E = \frac{1}{2}\int_{-\infty}^{\mu} d\omega \rho(\omega)\omega - 4t\sum_{\sigma}\langle a_{i\sigma}^{\dagger} d_{i\sigma}\rangle + \tfrac{1}{2}\mu n + \Delta n^{p}, \tag{41}$$

where $\rho(\omega)$ is the total LDOS of the trimer, and

$$\langle a_{i\sigma}^{\dagger} d_{i\sigma}\rangle = -\frac{1}{\pi}\int_{-\infty}^{\mu} d\omega \mathrm{Im} G_{ad}^{\sigma}(\omega + i\delta). \tag{42}$$

An equivalent expression for the one-band Hubbard model has been utilized in Ref. 40, where the derivation is indicated.

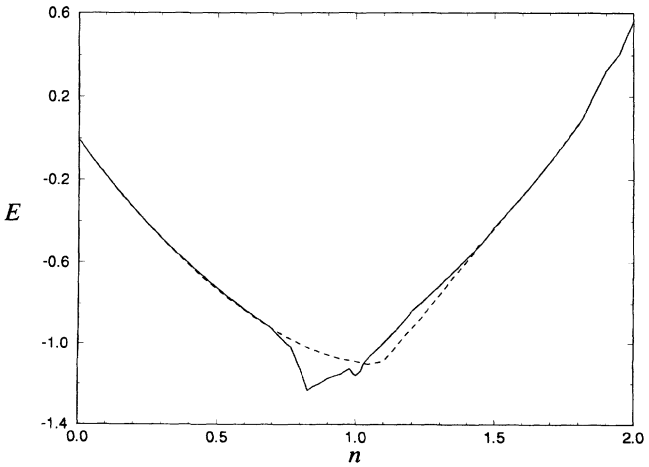

FIG. 10. Internal energy per trimer as a function of the hole number in the PM (dashed) and AF (solid) phases.

Figure 10 shows the energy E as a function of n. One can see that the AF phase is stable between $n \approx 0.70$ and $n \approx 1.02$. The stoichiometric concentration $n = 1.00$ corresponds to a local minimum of $E(n)$. In the region where the two curves coincide, the PM phase should be stable, because one can no longer justify the introduction of the infinitesimal magnetic field h that gave rise to the AF phase.

IV. CONCLUSION

An approximate Green function formalism has been developed for the three-band Hubbard model. The Hamiltonian is divided in such a way that it preserves in the unperturbed part, i.e., inside the trimers, part of the competition between local correlations and itineracy.

The emerging physical picture is the following: as particles fill the band structure shown in Fig. 2, its shape is continuously changed (Figs. 3 and 4) in order to account for the Coulomb repulsions U_p and U_d. One can identify the presence of the Zhang-Rice singlet band near the top of the CT gap. In the PM phase, this gap is only crossed by the chemical potential for $n \approx 1.10$, as indicated by the jump of $\mu(n)$ in Fig. 5 (dashed line). The insulating character of the stoichiometric compound is verified in the AF phase (solid line), where the discontinuity is shifted to $n = 1.00$. With reference to the stoichiometric densities of states in Fig. 7, one observes that in-gap bands are formed upon carrier doping. For a larger amount of doping, these bands eventually collapse with the nearest ones, assuming the form of Figs. 2 and 4 (for electron and hole doping, respectively).

There is an intrinsic asymmetry between electron and hole doping. The critical concentrations for the disruption of antiferromagnetic order are $n \approx 1.02$ for hole doping and $n \approx 0.70$ for electron doping. For electron doping, it is interesting to note that, in the range of concentrations $n \approx 0.70$ to $n \approx 0.97$, the chemical potential is not located at the gap states but near the singularity in the lower band, as illustrated in Fig. 8. In the AF phase, doped holes prefer the O sites, in contradistinction to what occurs in the PM phase. It is worth remarking that the critical concentrations are sensitive to the interpolation scheme adopted [Eq. (13)], and thus constitute an estimate for the model. An improvement can be achieved by introducing variational parameters for the concentrations of the two trimer species which minimize the internal energy.

The important role of the direct hopping t_{pp} between nearest-neighbor oxygen ions has been put into evidence in Ref. 23. One predictable effect of its inclusion in our model Hamiltonian is to produce a broadening of the δ functions appearing in the nonbonding part of the LDOS, with a corresponding decrease in the magnitude of the CT gap. The introduction of the Coulomb repulsion U_{dp} between neighboring copper and oxygen ions can also be explored by the present technique in the search for an electronic local pairing mechanism.

ACKNOWLEDGMENTS

B.H.B. would like to thank M. A. Gusmão, A. M. Oleś, and J. J. Rodríguez-Núñez for useful discussions. This work was supported by Brazilian agency CNPq (Conselho Nacional de Desenvolvimento Científico e Tecnológico) and French-Brazilian agreement CAPES-COFECUB. Numerical work has been performed in the Cray YMP-2E of the Centro Nacional de Supercomputação da Universidade Federal do Rio Grande do Sul.

APPENDIX

In Eqs. (38–40), we make use of

$$\lambda_0 = 2A' - g_+^{\sigma} A, \tag{A1}$$

$$\lambda_1 = 2B' - g_+^{\sigma} B, \tag{A2}$$

$$\lambda_2 = -g_+^{\sigma} C, \tag{A3}$$

$$\lambda_0' = g_{dd}^{*\sigma} + t^4 (g_{dd}^{\bar{\sigma}})^2 g_+^{*\sigma} \left[2(g_{ad}^{*\sigma})^2 + g_{dd}^{*\sigma} g_-^{*\sigma}\right], \tag{A4}$$

$$\lambda_1' = 2t^2 g_{dd}^{\bar{\sigma}} \left[(g_{ad}^{*\sigma})^2 + g_{ac}^{*\sigma} g_{dd}^{*\sigma}\right], \tag{A5}$$

$$\lambda_0'' = 4 g_{ad}^{\sigma} g_{ad}^{*\sigma} - FA, \tag{A6}$$

$$\lambda_1'' = 4t^2 g_{ad}^{\sigma} g_{ad}^{*\sigma} g_{dd}^{\bar{\sigma}} g_+^{*\sigma} - FB, \tag{A7}$$

$$\lambda_2'' = -FC, \tag{A8}$$

$$A = 1 + 4t^4 (g_{ad}^{\bar{\sigma}})^2 \left[(g_{ad}^{*\sigma})^2 - g_{aa}^{*\sigma} g_{dd}^{*\sigma}\right] - t^4 (g_{dd}^{\bar{\sigma}})^2 g_+^{*\sigma} g_-^{*\sigma} + 4t^6 (g_{ad}^{\bar{\sigma}})^2 g_{dd}^{\bar{\sigma}} g_+^{*\sigma} \left[2(g_{ad}^{*\sigma})^2 + g_{dd}^{*\sigma} g_-^{*\sigma}\right], \tag{A9}$$

$$B = 2t^2 (g_{dd}^{*\sigma} g_{ac}^{\bar{\sigma}} + g_{dd}^{\bar{\sigma}} g_{ac}^{*\sigma}) + 2t^4 \left[2(g_{ad}^{*\sigma})^2 + g_{dd}^{*\sigma} g_-^{*\sigma}\right] \times \left\{2(g_{ad}^{\bar{\sigma}})^2 + t^2 g_{dd}^{\bar{\sigma}} g_+^{*\sigma} \left[2(g_{ad}^{\bar{\sigma}})^2 + g_{ac}^{\bar{\sigma}} g_{dd}^{\bar{\sigma}}\right]\right\}, \tag{A10}$$

$$C = 4t^4 \left[(g_{ad}^{*\sigma})^2 + g_{ac}^{*\sigma} g_{dd}^{*\sigma}\right] \left[(g_{ad}^{\bar{\sigma}})^2 + g_{ac}^{\bar{\sigma}} g_{dd}^{\bar{\sigma}}\right], \tag{A11}$$

$$D = -4t^2 g_{ad}^{*\sigma} g_{ad}^{\bar{\sigma}} \left[1 + t^2 g_{dd}^{\bar{\sigma}} g_+^{*\sigma}\right], \tag{A12}$$

$$A' = g_{aa}^{*\sigma} + 2t^4 g_+^{*\sigma} (g_{ad}^{\bar{\sigma}})^2 \left[2(g_{ad}^{*\sigma})^2 + g_{dd}^{*\sigma} g_-^{*\sigma}\right], \tag{A13}$$

$$B' = A' - g_{aa}^{*\sigma} - 2t^2 \left[(g_{ad}^{*\sigma})^2 - g_{aa}^{*\sigma} g_{dd}^{*\sigma}\right], \tag{A14}$$

$$F = 2(g_{ad}^{\sigma})^2 + g_{dd}^{\sigma} g_-^{\sigma}, \tag{A15}$$

$$g_{\pm} = g_{ac} \pm g_{aa}, \tag{A16}$$

and r, s, u, and v are the roots of

$$P' = \left[Cx^2 + (B+D)x + (A+D)\right] \times \left[Cx^2 + (B-D)x + (A-D)\right]. \tag{A17}$$

[1] D. Vaknin *et al.*, Phys. Rev. Lett. **58**, 2802 (1987).
[2] J. M. Tranquada *et al.*, Phys. Rev. Lett. **60**, 156 (1988).
[3] V. J. Emery, Phys. Rev. Lett. **58**, 2794 (1987).
[4] C. M. Varma, S. Schmitt-Rink, and E. Abrahams, Solid State Commun. **62**, 681 (1987).
[5] J. H. Brewer *et al.*, Phys. Rev. Lett. **60**, 1073 (1988).
[6] Y. Kitaoka *et al.*, Physica C **153-155**, 733 (1988).
[7] Y. J. Uemura *et al.*, Physica C **162-164**, 857 (1989).
[8] R. L. Lichti *et al.*, Physica C **180**, 358 (1991).
[9] A. M. Oleś and J. Zaanen, Phys. Rev. B **39**, 9175 (1989).
[10] J. Dutka and A. M. Oleś, Phys. Rev. B **42**, 105 (1990); **43**, 5622 (1991).
[11] F. Yndurain and G. Martinez, Phys. Rev. B **43**, 3691 (1991).
[12] J. Brinckmann and N. Grewe, Z. Phys. B **84**, 179 (1991).
[13] C. A. Balseiro *et al.*, Phys. Rev. Lett. **62**, 2624 (1989).
[14] H. Romberg *et al.*, Phys. Rev. B **42**, 8768 (1990).
[15] J. W. Allen *et al.*, Phys. Rev. Lett. **64**, 595 (1990).
[16] C. T. Chen *et al.*, Phys. Rev. Lett. **66**, 104 (1991).
[17] T. Watanabe *et al.*, Phys. Rev. B **44**, 5316 (1991).
[18] H. Eskes, M. B. Meinders, and G. A. Sawatzky, Phys. Rev. Lett. **67**, 1035 (1991).
[19] F. C. Zhang and T. M. Rice, Phys. Rev. B **37**, 3759 (1988).
[20] W. Zhang and K. H. Bennemann, Phys. Rev. B **45**, 12 487 (1992).
[21] J. J. Rodríquez-Núñez, R. Medina, and P. Silva (unpublished).
[22] M. E. Simón, M. Baliña, and A. A. Aligia (unpublished).
[23] J. J. Rodríquez-Núñez and H. Beck, J. Phys. Condens. Matter **5**, L613 (1993).
[24] E. Dagotto *et al.*, Phys. Rev. B **41**, 9049 (1990).
[25] W. Stephan and P. Horsch, Phys. Rev. Lett. **66**, 2258 (1991).
[26] E. Dagotto *et al.*, Phys. Rev. B **45**, 10 741 (1992).
[27] E. Dagotto, F. Ortolani, and D. Scalapino, Phys. Rev. B **46**, 3183 (1992).
[28] J. E. Hirsch, S. Tang, E. Loh, and D. J. Scalapino, Phys. Rev. Lett. **60**, 1668 (1988).
[29] C. A. Balseiro, A. G. Rojo, E. R. Gagliano, and B. Alascio, Phys. Rev. B **38**, 9315 (1988).
[30] W. H. Stephan, W. v. d. Linden, and P. Horsch, Phys. Rev. B **39**, 2924 (1989).
[31] G. Dopf *et al.*, Phys. Rev. Lett. **68**, 2082 (1992).
[32] R. T. Scalettar *et al.*, Phys. Rev. B **44**, 770 (1991).
[33] C. A. Balseiro, M. Avignon, and E. R. Gagliano, Solid State Commun. **72**, 763 (1989).
[34] S. Maekawa, Y. Ohta, and T. Tohyama, in *Physics of High Temperature Superconductors*, edited by S. Maekawa and M. Sato, Springer Series of Solid State Sciences Vol. 106 (Springer-Verlag, Berlin, 1992), p. 29.
[35] B. H. Bernhard and J. R. Iglesias, Phys. Rev. B **47**, 12 408 (1993).
[36] C. D. Daguspa and P. Pfeuty, J. Phys. C **14**, 717 (1981).
[37] J. Hubbard, Proc. R. Soc. London Ser. A **276**, 238 (1963).
[38] M. L. Kulić *et al.*, Phys. Lett. A **148**, 372 (1990).
[39] A. Beatrici and M. A. Gusmão (unpublished).
[40] Th. Pruschke, D. L. Cox, and M. Jarrell, Phys. Rev. B **47**, 3553 (1993).